J Sol-Gel Sci Technol (2012) 61:534–540
DOI 10.1007/s10971-011-2656-8

ORIGINAL PAPER

Synthesis of multielement ferrites and their silica composites

A. A. Rodríguez-Rodríguez · O. S. Rodríguez-Fernández · J. G. Osuna-Alarcón · Sagrario M. Montemayor

Received: 5 April 2011 / Accepted: 9 December 2011 / Published online: 17 December 2011

Abstract Ferrites of composition $M_{0.2}Co_{0.4}Zn_{0.4}Fe_2O_4$ with M = Cu^{2+}, Mn^{2+} and Ni^{2+} were prepared by citrate complex method. Later, their composites with silica have also been obtained by a simple route. The citrate complex precursors of multielement ferrites were characterized by FTIR spectroscopy and thermal analysis, been found a similar behavior for the three systems. The thermal treatment (at 400, 600 and 800 °C) of precursors gives, as result, the spinel type cubic ferrite pure when the ions substituted were copper and nickel; when manganese was used an hematite phase was obtained as contaminant at 800 °C. The presence of all ions involved and the particle size was corroborated by EDX analysis and measured from a TEM micrograph, respectively. The magnetic parameters related to magnetic properties, magnetization and coercivity, were different depending of the chemical composition of the ferrite and the thermal treatment temperature, as it was expected. At room temperature, the values obtained were near to those reported for Co-ferrite in bulk. The synthesis route of the composites $M_{0.2}Co_{0.4}Zn_{0.4}Fe_2O_4$-$SiO_2$, proposed in this work, gives as result magnetic nanoparticles in an amorphous silica matrix. Their magnetic properties were depending on weight percentage of the magnetic phase in the composite.

A. A. Rodríguez-Rodríguez · J. G. Osuna-Alarcón · S. M. Montemayor (✉)
Universidad Autónoma de Coahuila, V. Carranza esq. J. Cárdenas s/n, 25280 Saltillo, Coahuila, Mexico
e-mail: sagrario.martinez.montemayor@uadec.edu.mx; smmontemayor@gmail.com

O. S. Rodríguez-Fernández
Centro de Investigación en Química Aplicada, Blvd. Enrique Reyna Hermosillo No. 140, 25253 Saltillo, Coahuila, Mexico

Keywords Multielement ferrites · Ferrites-silica composites · Magnetic properties · Sol–gel · Mechanosynthesis

Abbreviations
CA Citric acid
EG Ethylene glycol

1 Introduction

Traditionally soft ferrites (MFe_2O_4) have been used in a broad variety of applications such as magnetic storage devices, core materials for power transformers, antenna rods, loading coils, etcetera [1]. The use of chemical routes for their synthesis have allowed to obtain ferrites in the nanometric scale, which present magnetic, electric, catalytic and mechanical properties outstandingly improved with respect to the existing materials [2, 3]. Nanometric soft ferrites are nowadays used, moreover, as microwave absorbents, magnetically guided drug deliverers, ferrofluids, multilayer chip inductors, electromagnetic interference filters, etc. [4]. An additional advantage of some chemical routes is the possibility to control the stoichiometry of the products [5]. In this sense, multielement ferrites, principally those based on Ni–Zn or Mn–Zn have been synthesized and have shown prominent properties [6, 7]. Actually, exist a growing interest in synthesize ferrites substituted by more than two ions because they have shown, in some cases, coupling phenomena and interactions between electrical current and magnetism [8], which is interesting from a theoretical point of view, and give place to many potential future applications, e.g. magnetologic devices [9], photonic systems [10], spintronic devices

[11], biomedical systems [6, 12] by mention some. An important fact is the trend of small particles to agglomerate, in order to reduce the energy associated with their high surface area. To minimize this, dispersing or embedding the nanoparticles into a silica matrix has been a successful method [12]. Some advantages of synthesizing multielement ferrites into a silica matrix are: chemical stability, strong magnetization, low coercivity, biological or electronic compatibility provided by the good possibility of functionalize the silica, etc.

For all these reasons, we have carried out the synthesis of three different ferrites of $M_{0.2}Co_{0.4}Zn_{0.4}Fe_2O_4$ composition by the citrate complex method, and we have systematically studied the effect, on the magnetic properties, of the M substitution by different divalent ions (Cu^{2+}, Mn^{2+} or Ni^{2+}). Moreover, this paper reports a simple mechanochemical approach that provides a resolution of several important problems in the synthesis of magnetic nanoparticles-silica composites by Stöber process related to the necessity of silicate pretreatment and its slow kinetics [13].

2 Materials and methods

The chemical reagents used in this work were citric acid monohydrate, ethylene glycol, $Cu(NO_3)_2{\cdot}6H_2O$, $Mn(NO_3)_2{\cdot}6H_2O$, $Ni(NO_3)_2{\cdot}6H_2O$, $Co(NO_3)_2{\cdot}6H_2O$, $Zn(NO_3)_2{\cdot}6H_2O$, $Fe(NO_3)_3{\cdot}9H_2O$, tetraethylorthosilicate (TEOS), oleic acid, heptane, purchased from Aldrich. All chemicals were analytical grade (purity >99.9%) and used without further purification.

2.1 Synthesis of $M_{0.2}Co_{0.4}Zn_{0.4}Fe_2O_4$

In general the citric acid was mixed with ethylene glycol, at room temperature under magnetic stirring until a transparent solution was obtained, in a molar relation 1–4, respectively. Then appropriate amount of iron nitrate (2 mol), zinc nitrate (0.4 mol), cobalt nitrate (0.4 mol) and, finally, copper, manganese or nickel nitrate (0.2 mol) were added into the solution, one by one, in that order, ensuring the complete dissolution before add the next salt. Homogeneous citrate complex solutions were obtained. Every solution was heated at ~130 °C by 2 h to increase the viscosity as a consequence of the evaporation of solvent in excess and water produced by condensation reaction between citric acid and ethylene glycol. The precursors were casted on Petri dishes and treated at 130 °C by 72 h in an oven. Dark brown vitreous films were obtained and, then, grounded into powder and calcined at 400, 600 and 800 °C by 2 h under air atmosphere. A flowchart of this procedure is shown in Scheme 1.

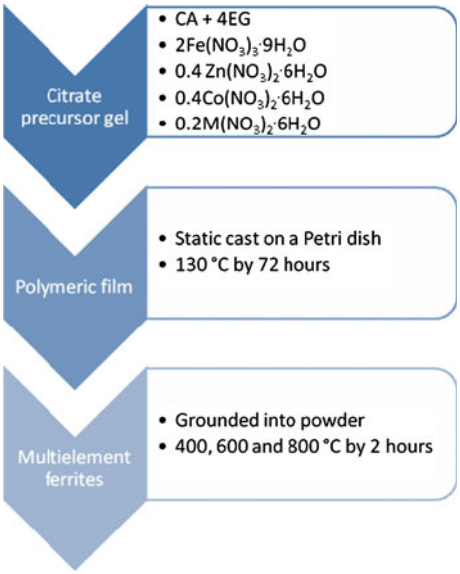

Scheme 1 Flowchart of $M_{0.2}Co_{0.4}Zn_{0.4}Fe_2O_4$ synthesis

2.2 Synthesis of $M_{0.2}Co_{0.4}Zn_{0.4}Fe_2O_4$-$SiO_2$ composites

The composites based on magnetic nanoparticles, $M_{0.2}Co_{0.4}Zn_{0.4}Fe_2O_4$ with M = Cu, Mn or Ni, and an amorphous silica matrix were produced by high energy ball milling. Into the vial were collocated: balls (~50 g), as milling medium; $M_{0.2}Co_{0.4}Zn_{0.4}Fe_2O_4$ (5 g), as magnetic nanoparticles; oleic acid (15 mL), as surfactant; and heptane (30 mL), as solvent. The vial and balls (15 mm) were made of agate. The blends were subjected to a rotational speed of 200 rpm by 2 h. During 1 h the sample was left in repose. This procedure was repeated 3 times. After this, 10 mL of TEOS were added to the blend and milled again at 200 rpm by 2 h with 1 h in repose by three times. Finally, the heptane excess was removed at 50 °C by 2 h in an oven.

2.3 Characterization techniques

The identification of citrate complexes and ester groups in the precursors were studied by FTIR spectroscopy, by transmission through KBr pellets containing about 1% of sample, using a Thermo-Nicolet/Nexus 470 spectrometer.

The thermal behavior of precursors was followed by thermogravimetric analysis, in a Shimadzu TGA-50, from 25 to 800 °C with a heating rate of 10 °C/min.

The crystalline phases were identified by XRD on a SIEMENS D-5000 powder diffractometer (25 mW, 35 kV) in the 10–80 2θ (°) range with a step of 0.02 °/s, using CuK_α radiation ($\lambda = 0.15418$ nm). The crystallite mean size was deduced from XRD line integral breath β using Scherrer's equation [14]. The particle size, crystallinity and composition of ferrite nanoparticles and composite

(ferrites-SiO_2) were characterized by high resolution transmission electron microscopy (HRTEM) coupled with energy-dispersive X-ray spectroscopy. A field-emission electron-source TEM (FEI-TITAN) was operated at 300 kV. The samples were deposited on a gold-grid-supported perforated transparent carbon foil.

The magnetic properties of the nanoparticles and their composites were measured, at 3 K and room-temperature, on a Quantum Design SQUID with VSM option. The magnetization values are given per gram of sample.

3 Results and discussion

FTIR spectra of precursors synthesized to obtain the multi-element ferrites, $M_{0.2}Co_{0.4}Zn_{0.4}Fe_2O_4$, present characteristic absorption bands similar even when the solutions were heated at 130 °C for 24, 48 or 72 h. Figure 1 shows the FTIR spectrum of the $Cu_{0.2}Co_{0.4}Zn_{0.4}Fe_2O_4$ precursor (130 °C/24 h) as an example. The broad band at ~3,400 cm^{-1} is related to the stretching vibration (ν) of O–H bonds present in the polyester obtained from the reaction between CA and EG, in metallic salts presence, and the EG in excess trapped into the polymeric chains. Thin bands at 1,650, 1,380 and 1,247 cm^{-1} are due to stretching modes (ν) of C = O and C–O when the carboxylate groups are bonded to metallic ions. Small signals at 895, 790 and 530 cm^{-1} are attributable to bending mode (δ) of the same bonds in the carboxylate groups. All this is supported by analogy with evidence from FTIR and NMR spectroscopy reported previously for similar systems [15, 16].

Figure 2 shows a characteristic thermogram (TGA) of the $M_{0.2}Co_{0.4}Zn_{0.4}Fe_2O_4$ precursors, in specific that obtained from $Mn_{0.2}Co_{0.4}Zn_{0.4}Fe_2O_4$ precursor (130 °C/72 h). As can be observed the precursors degrade through two critical steps. The first step of weight loss corresponds to the gradual evaporation of adsorbed water and EG trapped into polymeric network in the range of 25–300 °C. The second weight loss is due to a fast degradation of polyester (formed through a Fisher esterification reaction between CA and EG, the polymeric product is due to the functionality of the reagents used) which finish at ~320 °C. A total weight loss of ~60% was observed, for all samples, and attributed to organics present in the precursors. DTA curves (not included in this paper) show that first step is an endothermic reaction whereas the decomposition is an exothermic reaction. The absence of a second exothermic peak indicates that decomposition and crystallization occur simultaneously over the temperature range of 300–320 °C. So, thermal treatments from 400 °C are necessary and helpful to complete the ferrite crystallization process from the precursors synthesized.

Figure 3 shows, as an example, the XRD patterns of $Ni_{0.2}Co_{0.4}Zn_{0.4}Fe_2O_4$, obtained at 400, 600 and 800 °C. All the broad characteristic peaks associated to a spinel-type cubic structure [17], PDF 22-1086, appear except the XRD diagram corresponding to sample $Ni_{0.2}Co_{0.4}Zn_{0.4}Fe_2O_4$, at 400 °C, which shows only a broad maximum of low intensity.

In general, it is appreciable how the diffraction peaks become sharper as the treatment temperature increase, revealing the larger size of nanocrystals. A high temperature for Mn^{2+}, in that sample treated at 800 °C, produce an inhomogeneous sample (with its decomposition [18]) and the crystallization of Fe^{3+} in excess, as hematite (~30%W of Fe_2O_3 PDF 33-0664), in addition to spinel-type cubic structure. As can be observed in Table 1, where they are tabulated the composition, structural parameters and

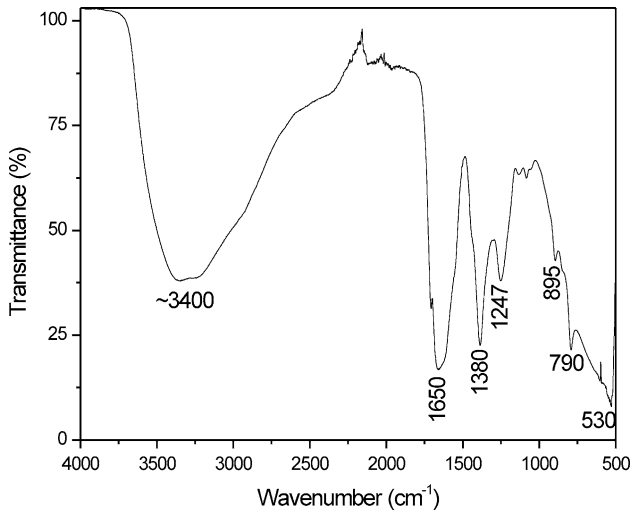

Fig. 1 FT-IR spectrum of $Cu_{0.2}Co_{0.4}Zn_{0.4}Fe_2O_4$ precursor (130 °C/24 h)

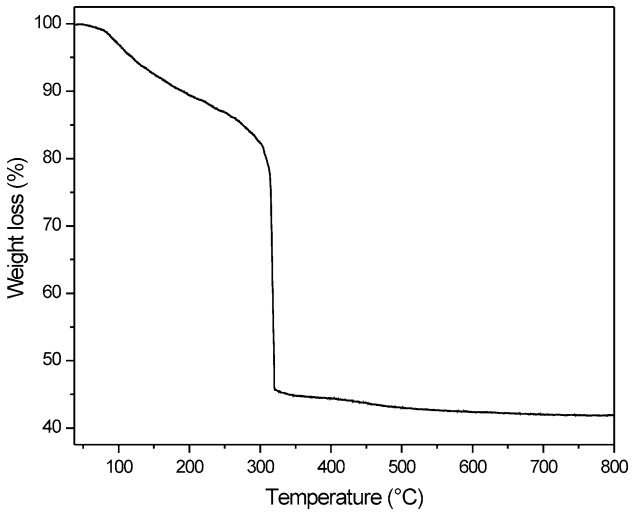

Fig. 2 TGA thermogram of $Mn_{0.2}Co_{0.4}Zn_{0.4}Fe_2O_4$ precursor (130 °C/72 h)

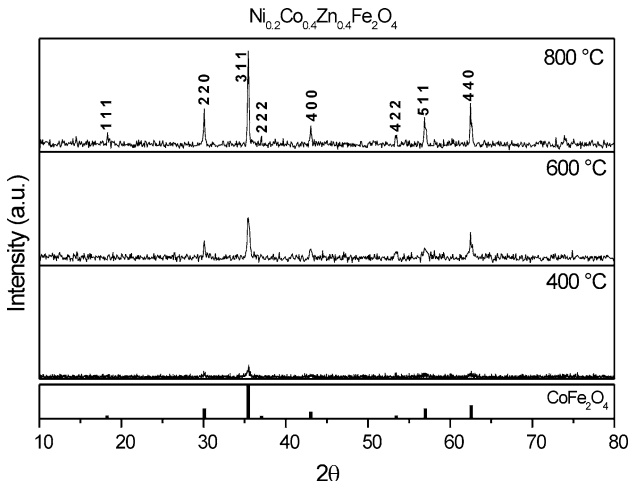

Fig. 3 XRD patterns of $Ni_{0.2}Co_{0.4}Zn_{0.4}Fe_2O_4$ obtained at 400, 600 and 800 °C (2 h)

average crystallite sizes. The lattice parameter *a* obtained for $Cu_{0.2}Co_{0.4}Zn_{0.4}Fe_2O_4$ and $Ni_{0.2}Co_{0.4}Zn_{0.4}Fe_2O_4$ (8.3964 Å) is between those reported values of 8.3919 and 8.4409 Å for $CoFe_2O_4$ and $ZnFe_2O_4$, respectively (PDF 22-1086 and 82-1049). By contrast, $Mn_{0.2}Co_{0.4}Zn_{0.4}Fe_2O_4$ shows a different lattice parameter value depending of the temperature. This could be attributed, again, to a lack of homogeneity in this sample as a consequence of a high temperature [18]. The crystallite size range calculated, using a Gaussian and Lorentzian peak shape of equal contribution on the most intense reflection ($h\ k\ l = \mathbf{3\ 1\ 1}$), vary from 13.6 to 63.8 nm. The increase of this value is a consequence, mainly, of the increase in the temperature of thermal treatment of the precursors. It is important to mention that the presence of all cations in the structure was corroborated by EDX analysis.

The room-temperature magnetization curves of the studied multielement ferrites, treated at 600 and 800 °C, display the typical ferrimagnetic behavior; with large saturation magnetization, in the range found for bulk Co-ferrite [19], although had less coercivity. As an example, Fig. 4 shows the magnetization curves of ferrites obtained at 600 °C. The ferrimagnetic nature is corroborated by the magnetization measurements under zero-field cooling conditions where a continuously increasing until 300 K is observed for $Cu_{0.2}Co_{0.4}Zn_{0.4}Fe_2O_4$, $Mn_{0.2}Co_{0.4}Zn_{0.4}Fe_2O_4$ or $Ni_{0.2}Co_{0.4}Zn_{0.4}Fe_2O_4$ [17]. In agreement with the difference observed in particle size, at 600 °C for the $Mn_{0.2}Co_{0.4}Zn_{0.4}Fe_2O_4$, shows a smaller saturation magnetization value than that reached for $Cu_{0.2}Co_{0.4}Zn_{0.4}Fe_2O_4$ and $Ni_{0.2}Co_{0.4}Zn_{0.4}Fe_2O_4$.

As its well known, low temperature magnetization measurements provide, at temperatures close to 0 K, information about distribution of cations within the spinel lattice. Namely, at 0 K, saturation magnetization directly reflects the difference in magnetization of the tetrahedral and the octahedral sublattices [17]. A lowest degree of inversion leads to largest values of saturation magnetization due to that magnetic moment per molecule of $CoFe_2O_4$ increases from 3 Bohr magnetons for inverse spinel to 7 Bohr magnetons for normal spinel [20]. Figure 5 shows hysteresis loops, measured at 3 K, of $M_{0.2}Co_{0.4}Zn_{0.4}Fe_2O_4$ composition nanoparticles obtained at 600 °C, of the three studied systems, $Cu_{0.2}Co_{0.4}Zn_{0.4}Fe_2O_4$ shows the largest saturation magnetization at 3 K (125.5 emu/g), which suggests a normal spinel type structure. Other reason for inferring a normal spinel is that the presence of M^{2+} in tetrahedral sublattice sites strongly reduces the coercivity from that would be expected if the M^{2+} was occupying octahedral sites [21]. The $Mn_{0.2}Co_{0.4}Zn_{0.4}Fe_2O_4$ nanoparticles (600 °C) present a similar behavior reaching a Ms value of 113.7 emu/g at 3 K. However, there is not difference in saturation magnetization values of $Ni_{0.2}Co_{0.4}Zn_{0.4}Fe_2O_4$, between that obtained at room temperature (74.9 emu/g) and 3 K (74.8 emu/g), which suggests an inverse spinel type structure. The distribution of

Table 1 Summary of the composition, structural parameters and crystallite size of ferrites $M_{0.2}Co_{0.4}Zn_{0.4}Fe_2O_4$ composition obtained at different temperatures by 2 h in an air atmosphere

Precursor	Crystalline phases	Lattice parameter (Å)	Crystallite size (nm)
CuCoZn-ferrite (°C)			
400	Spinel	8.3964 ± 0.0007	16.9 ± 0.015
600	Spinel	8.3964 ± 0.0004	28.9 ± 0.009
800	Spinel	8.3964 ± 0.0002	63.8 ± 0.004
MnCoZn-ferrite (°C)			
400	Spinel	8.4360 ± 0.0009	13.6 ± 0.019
600	Spinel	8.4096 ± 0.0006	19.2 ± 0.013
800	Spinel + hematite	8.4188 ± 0.0002	53.6 ± 0.005
NiCoZn-ferrite (°C)			
400	Amorphous	–	–
600	Spinel	8.3964 ± 0.0007	29.1 ± 0.015
800	Spinel	8.3964 ± 0.0003	50.1 ± 0.006

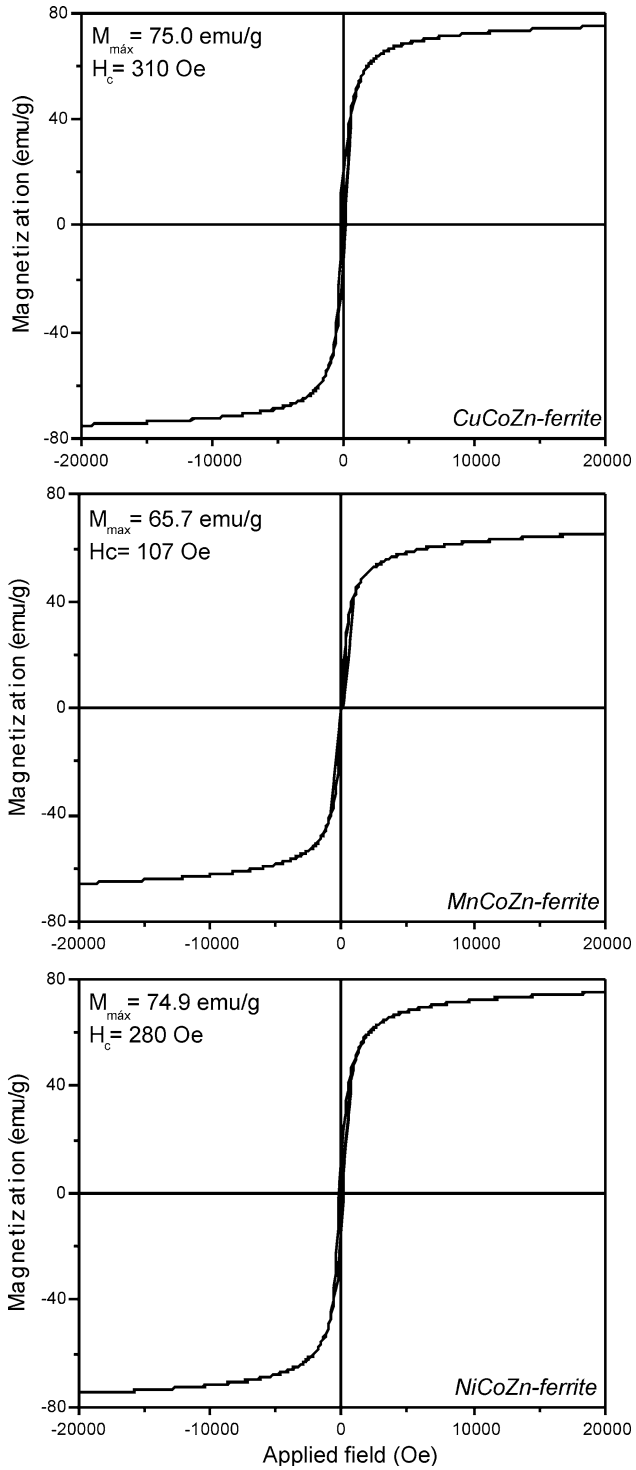

Fig. 4 Room temperature magnetization curves for $M_{0.2}Co_{0.4}Zn_{0.4}Fe_2O_4$ obtained at 600 °C

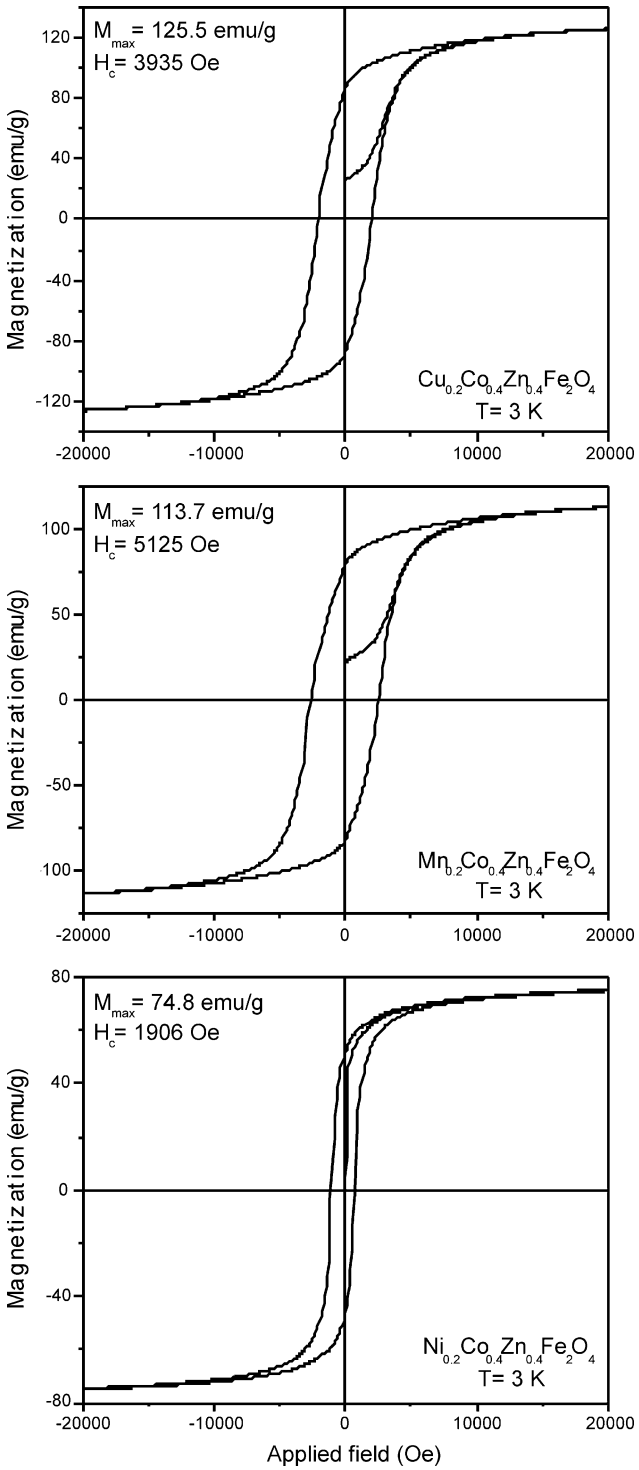

Fig. 5 M(H) at 3 K for $M_{0.2}Co_{0.4}Zn_{0.4}Fe_2O_4$

cations in the structure depends of many factors as synthetic method, heat treatment temperature, heat-duration time, cooling rate and, how occurs on this case, the nature of the substituents [22]. Indeed, to determine the percentage of each element over the tetrahedral or octahedral sites will be necessary to analyze the samples by Mossbauer or K-edge x-ray absorption spectroscopy.

Figure 6 shows the XRD patterns of the materials after the mechanical milling of $M_{0.2}Co_{0.4}Zn_{0.4}Fe_2O_4$ nanoparticles with TEOS, under the conditions reported in the

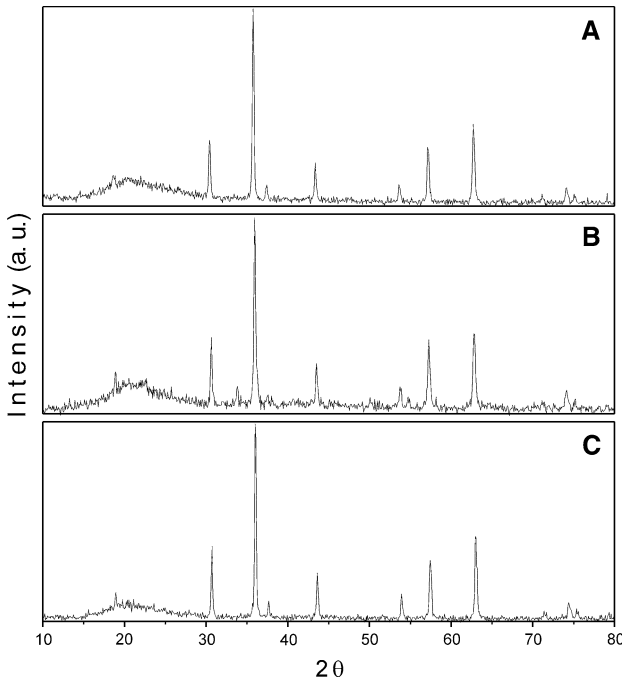

Fig. 6 XRD patterns for **a** $Cu_{0.2}Co_{0.4}Zn_{0.4}Fe_2O_4$-$SiO_2$, **b** $Mn_{0.2}Co_{0.4}Zn_{0.4}Fe_2O_4$-$SiO_2$ and **c** $Ni_{0.2}Co_{0.4}Zn_{0.4}Fe_2O_4$-$SiO_2$. Lower pattern 22-1086 PDF

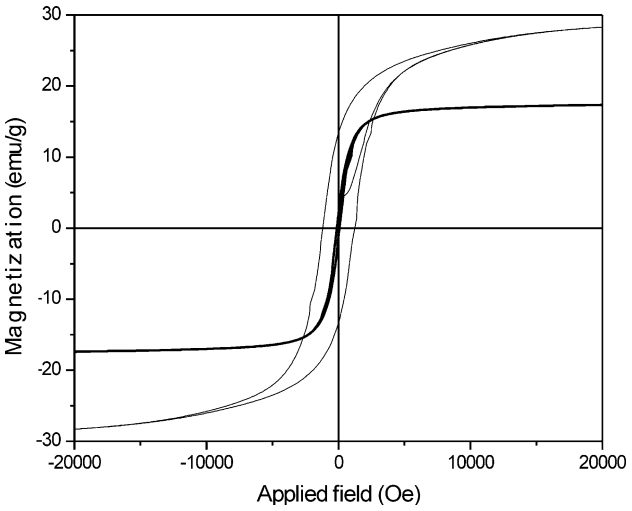

Fig. 8 M(H), at room temperature and 3 K, for $Cu_{0.2}Co_{0.4}Zn_{0.4}Fe_2O_4$-$SiO_2$

experimental part. The spinel phase expected is obtained in all the cases, as well as, a broad maximum of low intensity, at $\sim 20°$ (2θ), associated to the presence of SiO_2 in amorphous state.

TEM images corresponding to the $Cu_{0.2}Co_{0.4}Zn_{0.4}Fe_2O_4$ nanoparticles (left) and $Cu_{0.2}Co_{0.4}Zn_{0.4}Fe_2O_4$-$SiO_2$ composite (right) are shown in Fig. 7. After heating nanoparticles at 800 °C/2 h the images show agglomerated particles, which are still nanometer-sized, with the typical polygonal shape and an average diameter which increases up to around 70 nm in agreement with a progressive sintering process. These results imply that the heat energy supplied to the system not only induces the crystallization (observed by XRD) but also increases the surface energy of the particles favoring their aggregation. The procedure followed to obtain the composites does not induce the collapse of the magnetic phase as can be noticed at the right side image. Also, is evident, the presence of a silica matrix recovering the agglomerates.

The composites $M_{0.2}Co_{0.4}Zn_{0.4}Fe_2O_4$-$SiO_2$ show the ferrimagnetic behavior expected although the saturation magnetization values are decreased, with respect to that of $M_{0.2}Co_{0.4}Zn_{0.4}Fe_2O_4$, as a consequence of the non magnetic contribution of SiO_2. Two representative hysteresis loops, at room temperature and 3 K, are shown in Fig. 8 and the Ms and Hc values found for all systems are summarized in Table 2.

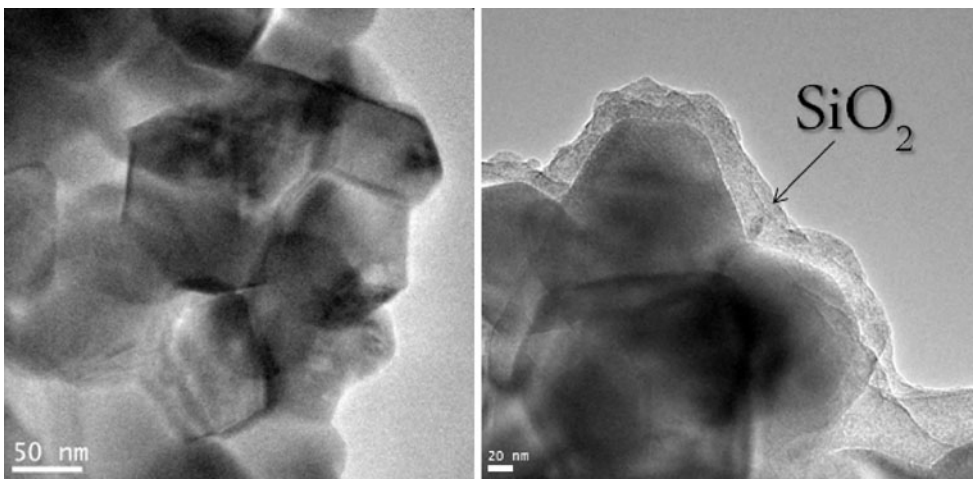

Fig. 7 TEM images of $Cu_{0.2}Co_{0.4}Zn_{0.4}Fe_2O_4$ nanoparticles (*left*) and $Cu_{0.2}Co_{0.4}Zn_{0.4}Fe_2O_4$-$SiO_2$ composite (*right*)

Table 2 Magnetic parameters of $M_{0.2}Co_{0.4}Zn_{0.4}Fe_2O_4$-$SiO_2$

Composite	Ms (emu/g)	Hc (Oe)
CuCoZn-ferrite-SiO_2		
Room temperature	17.4	196
3 K	28.3	2,500
MnCoZn-ferrite-SiO_2		
Room temperature	11.1	243
3 K	22.0	3,660
NiCoZn-ferrite-SiO_2		
Room temperature	13.3	245
3 K	13.4	2,575

4 Conclusions

The chemical route followed in this work lead to obtain the multielement ferrites, $Cu_{0.2}Co_{0.4}Zn_{0.4}Fe_2O_4$, $Mn_{0.2}Co_{0.4}Zn_{0.4}Fe_2O_4$ and $Ni_{0.2}Co_{0.4}Zn_{0.4}Fe_2O_4$, with nanometer particle size and magnetic properties in the range found for $CoFe_2O_4$ in bulk.

A simple mechanical milling route is useful in the obtaining of composites $M_{0.2}Co_{0.4}Zn_{0.4}Fe_2O_4$-$SiO_2$.

Acknowledgments Financial support from Secretaría de Educación Pública through of the project UACOAH-PTC-132 is gratefully acknowledged. A. A. Rodríguez-Rodríguez thanks the scholarship IOO-13-SNI-Estudiantes-2008-01.

References

1. Jiles D (1998) Introduction to magnetism and magnetic materials. Chapman and Hall, Iowa
2. Jalaly M, Enayati MH, Kameli P, Karimzadeh F (2010) Phys B 405:507–512
3. Tan X, Li G, Zhao Y, Hu C (2010) J Alloy Compd 493:55–63
4. Cui H, Jia Y, Ren W, Wang W (2010) J Sol Gel Sci Technol 55:36–40
5. Kakihana M (1996) J Sol Gel Sci Technol 6:7–55
6. Nam JH, Joo YH, Lee JH, Chang JH, Cho JH, Chun MP, Kim BI (2009) J Magn Magn Mater 321:1389–1392
7. Ju Y-W, Park J-H, Jung H-R, Cho S-J, Lee W-J (2008) Compos Sci Technol 68:1704–1709
8. Petracic O (2010) Superlattices Microstruct 47:569–578
9. Allwood DA (2005) Science 309:1688–1692
10. Lyubchanskii IL, Dadoenkova NN, Lyubchanskii MI, Shapovalov EA, Rasing Th (2003) J Phys D Appl Phys 36:R277–R287
11. Battle X, Labarta A (2002) J Phys D 35:R15–R42
12. Morel AL, Nikitenko SI, Gionnet K, Wattiaux A, Lai-Kee-Him J, Labrugere C, Chevalier B, Deleris G, Petibois C, Brisson A, Simonoff M (2008) ACS Nano 2:847–856
13. Conrad CF, Icopini GA, Yasuhara H, Bandstra JZ, Brantley SL, Heaney PJ (2007) Geochim Cosmochim Acta 71:531–542
14. Cullity BD (1978) Elements of X-ray diffraction. Addison-Wesley, USA
15. Montemayor SM, García Cerda LA, Torres-Lubián JR, Rodríguez-Fernández OS (2008) Mater Res Bull 43:1112–1118
16. Montemayor SM, García Cerda LA, Torres-Lubián JR, Rodríguez-Fernández OS (2008) J Sol Gel Sci Technol 42:181–186
17. Gyergyek S, Makovec D, Kodre A, Arcon I, Jagodic M, Drofenik M (2010) J Nanopart Res 12:1263–1273
18. Sharma P, Gupta A, Owens FJ, Inoue A, Rao KV (2004) J Magn Magn Mater 282:115–121
19. Smit J, Wijn HPJ (1959) Ferrites. Philips' Technical Library, Eindhoven
20. Kodama RH (1999) J Magn Magn Mater 200:359–372
21. Franco A, Zapf V (2008) J Magn Magn Mater 320:709–713
22. Gajbhiye NS, Balaji G, Bhattacharyya S, Ghafari M (2004) Hyperfine Interact 156/157:57–61